Large Eddy Simulation of Vented Deflagration

Pierre Quillatre,*,†,‡ Olivier Vermorel,† Thierry Poinsot,† and Philippe Ricoux‡

CERFACS, 42 Avenue Gaspard Coriolis, 31057 TOULOUSE Cedex 01, FRANCE, and TOTAL S.A., Tour Coupole, 92078 PARIS LA DEFENSE Cedex, FRANCE

E-mail: quillatre@cerfacs.fr

Abstract

In order to understand gas explosion phenomena in industrial buildings, a reduced-scale vented combustion chamber is investigated numerically. In this configuration, a flame is ignited in an initially quiescent flammable mixture and propagates past solid obstacles, generating a strong pressure increase. The aim of this numerical study is twofold: the first objective is to show how Large Eddy Simulation manages to reproduce the parameters of critical relevance for this multi-scale problem, in particular the overpressure generated during the flame propagation. The second objective is to highlight that, even if large to small-scale turbulence effects play a crucial role in the flame development and the resulting overpressure, it is also needed to correctly account for thermo-diffusive scale phenomena.

Introduction

Accidents due to gas explosions in industrial buildings such as offshore oil and gas producing platforms or oil storage facilities are a major safety issue. Although the primary objective is of

*To whom correspondence should be addressed
†CERFACS, 42 Avenue Gaspard Coriolis, 31057 TOULOUSE Cedex 01, FRANCE
‡TOTAL S.A., Tour Coupole, 92078 PARIS LA DEFENSE Cedex, FRANCE

course to prevent them, being able to understand the mechanisms which control them is a societal, economical and physical challenge of prime importance.

A typical explosion scenario begins with an ignition of a quiescent flammable mixture inside a confined or semi-confined area. Then the flame propagates and accelerates by interaction with obstacles (process equipment, structures, piping,...), generating a strong increase of pressure. This overpressure is the parameter of critical interest for safety studies since it can induce the destruction of the facilities involved. In order to understand explosions in confined and semi-confined areas, small to medium scale configurations of vented chambers are usually considered. Experimental[1–5] and numerical[6–8] studies of explosion have extensively been performed in order to point out the mechanisms involved in flame acceleration and pressure increase generation. Effects of geometric features or fuel type on this overpressure have also been studied.[9–11] Thanks to the growing computational power, Computational Fluid Dynamic (CFD) appears as an interesting alternative to experiments, which remain expensive and dangerous and bring limited material for diagnostic and understanding of explosions. Explosions are a typical multi-scale and multi-physics problem for which adapted numerical methods must be used. Up to now, safety related studies of explosions for industry have mainly been carried out using Unsteady Reynolds Averaged Navier-Stokes (URANS) methods.[12,13] However, the emergence of Large Eddy Simulation (LES) on massively parallel computers has considerably improved the ability to precisely simulate fully unsteady flows in complex geometries[11,14] and appears as a promising tool for explosion studies.

The ultimate objective of this research is to develop LES tools for realistic explosion cases where the sizes will be of the order of 10 to 100m and Reynolds numbers will be very large. To develop these LES tools and make sure that they can capture all phases of the flame development, the strategy is to begin with a smaller size experiment ($0.25m$) installed at the University of Sydney.[9] In this kind of configuration, the flow is largely turbulent during most part of the explosion. The large spectrum of turbulent scales present in this flow interacts with the flame and must be properly reproduced in order to accurately simulate the flame propagation in this environment. As

shown by Di Sarli *et al.*,[15–17] the predictive ability of LES strongly relies on the model implemented to take into account the flame-turbulence interaction. It is well known that the role played by the combustion sub-model is dependent on both, the grid resolution used and the combustion regime experienced by the propagating flame. However, the main aim of the present paper is to point out that, in LES, in addition to the importance to account for large to small-scale turbulent combustion effects, it is also needed to correctly account for thermo-diffusive scale phenomena. Reaching a correct reproduction of all these multi-scale phenomena is the prerequisite in order to accurately predict the global quantities of critical interest for safety related studies, in particular the overpressure generated in the chamber.

Test case

The configuration studied in this work was set up at the University of Sydney.[9] It consists in a square cross section premixed combustion chamber (25cm x 5cm x 5cm) with solid obstacles. The obstacles consist in three removable turbulence generating grids and one fixed central obstacle, as shown in Fig. 1 (left). The bottom end of the chamber is closed and the top end is opened out to the atmosphere. The vessel is initially filled with a premixed mixture of air and fuel at atmospheric pressure and temperature. Three different fuels are available: CNG (88% CH_4) at equivalence ratio $\Phi = 1$, LPG (95% C_3H_8) at $\Phi = 1$, and H_2 at $\Phi = 0.7$. The explosion scenario begins with an ignition of the quiescent premixed mixture at the closed end of the chamber. Ignition is followed by a laminar propagation phase and then an interaction with solid obstacles. When touching the obstacles, the initially laminar flame gets wrinkled and becomes a turbulent flame propagating at high speed. Additional details of the setup may be found in Masri *et al.*[9]

As mentioned earlier, the turbulence generating grids can be added or removed so that several configurations can be studied. Three configurations are studied here, where the number of grids is progressively increased from one to three, located farthest from the ignition point. Illustrations of the investigated configurations can be found in Fig. 1 (right). Two major aspects can therefore be

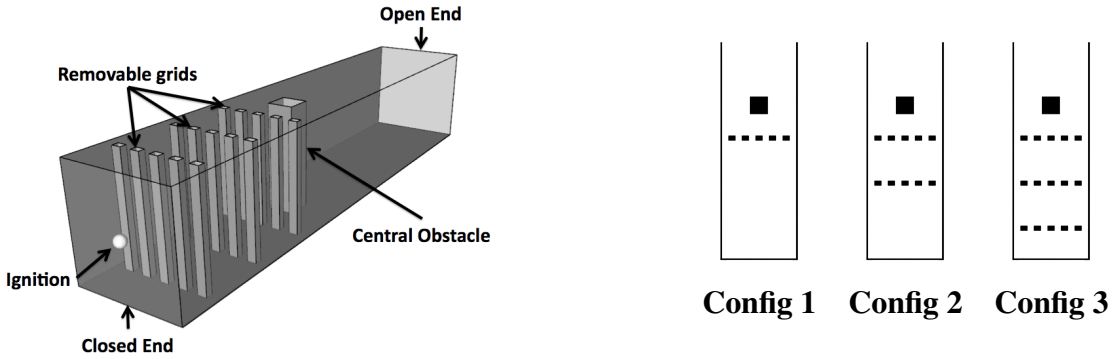

Figure 1: **Left:** Explosion chamber configuration of Masri *et al.*[9] The vessel is orientated vertically in the experiment : the bottom end of the vessel is on the left of the figure and the top end on the right. **Right:** Classification of the studied configurations.

studied using this experimental configuration:

- the influence of the fuel on the overpressure;
- the influence of the geometric features on the flame propagation and the resulting overpressure.

Numerical methods for explosion phenomena

Explosions are a multi-physics problem which requires to account for chemical kinetics, fluid flow, turbulence, wall phenomena and acoustics considering that all these phenomena, which occur over a large range of scales, are strongly coupled. The numerical method must thus be able to take into account all these scales. Explosions are consequently a typical multi-scale problem (Fig. 2). Chemical reactions taking place in flames occur in very thin fronts, typically less than 100 microns, and their kinetics is controlled by thermo and mass diffusive effects across these flame fronts. The smallest turbulent structures can reach less than 10 microns while the largest scales of the flow correspond to vortices with sizes of the order of the building size (10 to 100 m).

In order to reproduce explosion phenomena, various numerical approaches are available to solve the compressible reactive Navier-Stokes equations. These methods mainly differ by the way

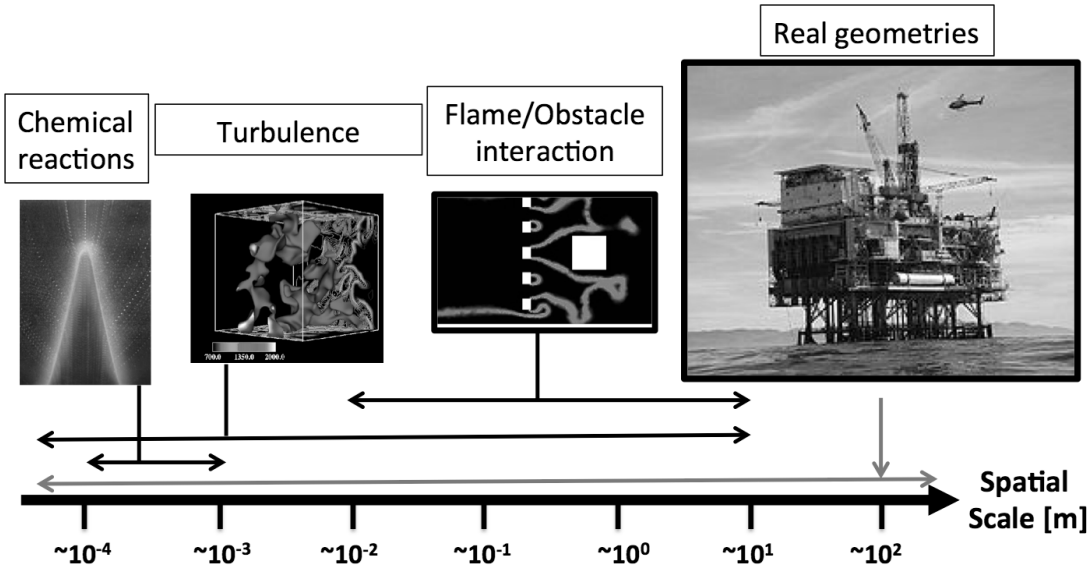

Figure 2: multi-scale aspect of explosion phenomena.

turbulence is accounted for:

- Direct Numerical Simulation (DNS) is a bruteforce approach: all turbulent scales are resolved in space and time. This method requires meshes with a cell size smaller than the smallest turbulent scale which is the Kolmogorov scale. For explosion configurations, this would consequently lead to meshes of several hundreds of billion points which is not affordable with the current CPU power. This method is in practice dedicated to academic configurations (e.g. Homogeneous Isotropic Turbulence), in very simple and small configurations.[18]

- Currently, CFD codes used for safety studies mainly rely on URANS methods.[12] This is a statistic approach where only averaged values are resolved, consequently considerably reducing the CPU cost. However, all turbulent scales have to be modeled, which can potentially lead to errors on their prediction.

- The emergence of Large Eddy Simulation (LES) on massively parallel computers has considerably improved the ability to precisely simulate fully unsteady flows in complex geome-

tries.[19,20] Indeed, the LES technique is a filterered approach which relies on a scale analysis of the turbulence: according to Kolmogorov,[21] turbulence may be considered in a fractal way where the smallest scale eddies energy can be deduced from the larger ones. LES method relies on this statement: the energetic largest turbulent scales are explicitly computed on the mesh points while the smallest are modeled from the resolved large scales. The overall model contribution in LES is thus reduced compared to (U)RANS methods where all turbulent scales are modeled. If the cell size is small enough, the model contribution naturally tends to zero and LES degenerates towards DNS. These properties allow a priori a better description of turbulent flows even though it requires more computational time. It is also worth noting that, by construction, LES is expected to be much less mesh dependent than (U)RANS as far as the LES cut-off length falls inside the inertial range of the energy spectrum.

LES has already shown its ability to give more reliable predictions than URANS in unsteady complex configurations such as piston engines[19] or gas turbines[20] which present many analogies with gas explosions in terms of turbulent combustion or confinement.

The LES solver used in this study is the AVBP code.[22,23] AVBP solves the unsteady compressible and reactive Navier-Stokes equations on unstructured grids. The present simulations are performed with a finite volume Lax-Wendroff convective scheme.[24] Navier-Stokes Characteristic Boundary Conditions (NSCBC)[25] are used at the outlet of the plenum which is located at the open end of the chamber in order to mimic the atmosphere. The solid walls that represent the obstacles and the explosion chamber are adiabatic non-slip walls.

As it has been mentioned, effects smaller than the mesh size have to be modeled:

- Sub-grid scale turbulence is modeled by the WALE viscosity based model.[26]

- When dealing with turbulent combustion configurations, another aspect of modeling is to be able to handle flame fronts which are generally much thinner than the cell size. If the flame structure is not resolved, it cannot be computed. For combustion, no theory enables to predict flame properties from large scales since combustion is inherently controlled by molecular processes. A method similar to LES for turbulence consequently cannot be applied. However, combustion theory[27] tells us how flame fronts can be thickened in space by a factor $\mathscr{F}$ and still propagate at the same speed. Here the Thickened Flame method[28] (TFLES) allows to make these fronts large enough to be resolved on the mesh. Flame-turbulence interaction at sub-grid scale is reproduced by multiplying the resolved reaction rate by an efficiency factor $\mathscr{E}$ which models the loss of wrinkling due to flame thickening. $\mathscr{E}$ is defined from the formulation of Colin *et al.*[28] as the ratio of sub-grid scale flame front wrinkling Ξ_Δ between a non-thickened and a thickened flame:

$$\mathscr{E} = \frac{\Xi_\Delta(\delta_l^0)}{\Xi_\Delta(\mathscr{F}\delta_l^0)} \tag{1}$$

where δ_l^0 is the laminar flame thickness of the non-thickened flame. The sub-grid scale flame front wrinkling Ξ_Δ is defined as:

$$\Xi_\Delta = 1 + \beta \frac{2ln(2)}{3c_{ms}[Re_t^{1/2} - 1]} \Gamma(\frac{\Delta}{\delta_l^0}, \frac{u'_\Delta}{S_l^0}) \frac{u'_\Delta}{S_l^0} \tag{2}$$

with $\Gamma(\frac{\Delta}{\delta_l^0}, \frac{u'_\Delta}{S_l^0}) = 0.75exp[-\frac{1.2}{[u'_\Delta/S_l^0]^{0.3}}](\frac{\Delta}{\delta_l^0})^{2/3}$, Δ the filter size, Re_t a Reynolds number based on an estimation of the turbulent integral length scale L_T ($L_T = 5.10^{-3}$), $\beta = 0.3$ and $c_{ms} = 0.28$. Note that this set of parameters has been kept constant for all the simulations presented in this paper.

- In the context of LES, due to their prohibitive computational cost, integration of detailed kinetics is impossible. In our work, chemistry is modeled by reduced schemes.[29] Thus, only the principal species and reactions are considered. Several one-step and two-step reduced

schemes have been developed for this work. Details on these schemes and their impact on the results are given in section “Results sensitivity to LES sub-models”.

- Ignition processes are very complex (energy transfer by laser to gas, plasma formation, shock waves, ...) and their modeling is a task that extends far beyond the scope of this study. In order to avoid this part of modeling, calculations are consequently initialized by a small sphere of burnt gases (radius 1cm) at the ignition point which is sufficiently strong to initialize the combustion process without any transient phase.

LES simulations were carried out on meshes of 20 millions tetrahedra with a typical cell size of 0.5 mm in the chamber. This mesh density has been chosen in order to ensure that the flame, even thickened, remains thinner than the distance between the bars of the baffle plate.

Results

The aim of this section is to check the ability of LES to simulate flame propagation past repeated obstacles and capture the critical physical quantity related to safety related studies, i.e. the overpressure generated in the chamber. Besides the understanding of explosion phenomena using LES results, a particular interest is brought to the influence of the fuel and of the number of turbulence generating grids. Finally, the focus is on the sensitivity of LES results to the sub-models used to reproduce small-scale chemistry and thermo-diffusive effects.

Phenomenological study

The primary objective of this section is to understand the phenomena occurring in explosions and to highlight the mechanisms responsible for the pressure increase. Results from LES of Config 2 are investigated in order to understand the typical flame behavior during the explosion.

Figure 3 shows LES images of flame propagation compared with experiments. In the early stage of propagation, the flame is laminar and develops with a hemispherical shape, then it transitions to a "finger" shape when it approaches the walls, still being laminar. This long laminar phase

controls the flame shape and strength just before it touches the obstacles. Finally, the flame front hits the obstacles, generating strong turbulence which accelerates the flame. All phases of flame propagation observed in experiments are qualitatively well reproduced by LES. The time interval between two successive images being kept constant between experiments and LES, this highlights that the simulation correctly reproduces the flame arrival time even though the fourth LES image shows a slightly faster flame acceleration than experiments.

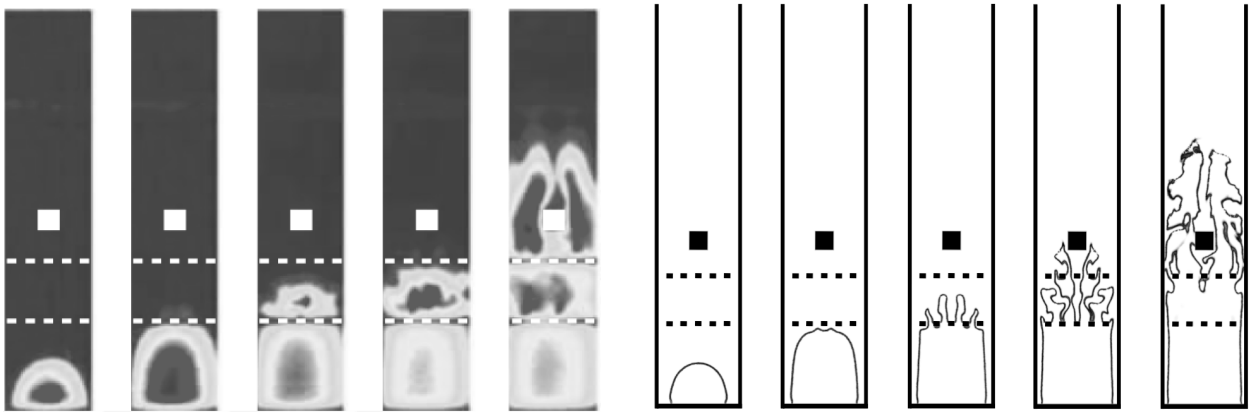

Figure 3: Images of flame propagation in Config2 using C_3H_8. Left: experimental video captured images (false colorized) extracted from Gubba *et al.*[6] Right: LES images (colored by reaction rate). - Time intervals between two successive images are kept constant between experiments and LES.

As mentioned earlier, the explosion induces a large pressure increase in the chamber which is the parameter of critical interest for safety related studies. Here we propose to investigate the mechanisms responsible for this increase using the LES results.

Although turbulent combustion flows are inherently controlled by small-scale physics (chemistry processes, interaction with turbulence, diffusive effects...), pressure increase in the chamber can be explained from a more global point of view, considering quantities integrated in the whole chamber. As explained by Di Sarli *et al.*,[8] the pressure increase observed in the chamber is due to the competition between two opposite phenomena: the combustion rate and the venting rate. On the one hand, the burnt gases accumulated inside the chamber by combustion processes have a lower density than the fresh gases they replace and consequently take up a bigger volume, inducing

a pressure increase. On the other hand, gases exhausting through the vent opening contribute to decrease the pressure. Working on a volume balance, a fine diagnostic has been set up in order to understand and highlight the mechanisms responsible for the pressure increase inside the chamber.

First, the venting rate $\dot{V}_{vent}$ is simply defined as the volume flow exhausting from the chamber:

$$\dot{V}_{vent} = \int_{S_{outlet}} U_n dS \tag{3}$$

where S_{outlet} is the section area of the chamber outlet and U_n is the velocity normal to this section.

Considering that the fresh gases (density ρ_f) which have been replaced by burnt gases (density ρ_b) took up a volume $V_f = \rho_b/\rho_f V_b$, the combustion rate $\dot{V}_{comb}$ can be written as the variation of the burnt gases volume minus the variation of the consumed fresh gases:

$$\dot{V}_{comb} = \frac{\partial V_b}{\partial t} - \frac{\partial V_f}{\partial t} = \frac{\partial V_b}{\partial t}(1 - \rho_b/\rho_f) \tag{4}$$

The variation of the burnt gases volume can be obtained from the mass reaction rate of any combustion product, here H_2O:

$$\frac{\partial V_b}{\partial t} = \frac{\dot{\omega}_{H_2O}}{\rho_b Y^b_{H_2O}} \tag{5}$$

where ${Y_{H_2O}}^b$ is the H_2O mass fraction in the burnt gases and $\dot{\omega}_{H_2O}$ is the production rate of species H_2O integrated over the whole chamber.

When $\dot{V}_{comb} > \dot{V}_{vent}$, the created volume is larger than the volume exhausting the chamber and the pressure increases. When $\dot{V}_{comb} < \dot{V}_{vent}$ the trend is opposite and the pressure decreases. Figure 4 (top) compares $\dot{V}_{comb}$ and $\dot{V}_{vent}$ to the overpressure (bottom) extracted from the LES results. We can notice the perfect match between the change of sign of $\dot{V}_{comb} - \dot{V}_{vent}$ and the maximum of overpressure around $T = 12ms$ (first vertical dotted line). Beyond the peak of overpressure,

acoustic reflections inside the chamber are also reproduced by this diagnostic. Arrows referenced as g2, g3, Obs and Out, respectively refer to the time at which the flame reaches the turbulence generating grids number 2, number 3, the central obstacle and the chamber outlet.

Thanks to this diagnostic, a first scenario of the explosion may be developed. In a first time, before hitting the obstacles, the flame is laminar and the combustion rate remains relatively low so that the "additional" volume created by the combustion process can correctly be exhausted through the vent opening. Then, following the contact with obstacles, the combustion rate strongly increases whereas these same obstacles constrain the flow which cannot properly exhaust from the chamber. The delay between these two phenomena induces the pressure increase. After the first overpressure peak, the flame reaches the chamber outlet and the combustion rate stops increasing. However, fresh gases which have been trapped in recirculation zones behind obstacles and in the corners of the chamber keep on burning, consequently maintaining the combustion rate. In the same time, acoustic reflections modify the venting rate and make the overpressure oscillate toward an equilibrium state at $P = P_{atm}$ alternating $\dot{V}_{comb} > \dot{V}_{vent}$ and $\dot{V}_{comb} < \dot{V}_{vent}$. These oscillations are reproduced in agreement with the frequency observed in experiments.

Numerical accuracy

As mentioned previously, all simulations were performed on the same mesh compound of 20 millions tetrahedral with a typical cell size of 0.5mm inside the chamber. An important point is to be able to estimate the quality of the results and especially to check if this resolution is adequate or not.

A first indication is to measure the respective contribution of the resolved and sub-grid scale parts of the combustion rate. Figure. 5 shows the contribution of the resolved part defined as the ratio between the resolved part of the reaction rate $\dot{\omega}_{res}$ and the total reaction rate $\dot{\omega}_{tot}$ when the

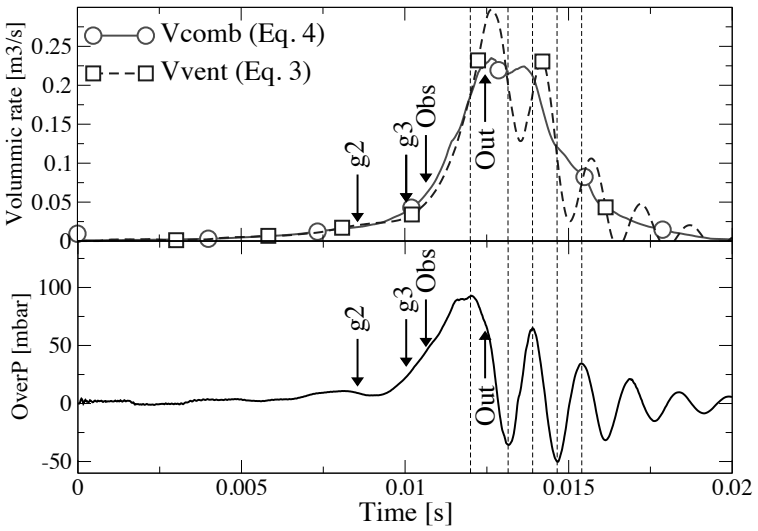

Figure 4: **Up** : Comparison between combustion rate $\dot{V}_{comb}$ and venting rate $\dot{V}_{vent}$ in fonction of time. **Bottom** : Overpressure inside the chamber in function of time.

flame interacts with the central obstacle:

$$\eta = \frac{\dot{\omega_{res}}}{\dot{\omega_{tot}}} = 1 - \frac{\dot{\omega_{sgs}}}{\dot{\omega_{tot}}} \tag{6}$$

with $\dot{\omega_{sgs}}$ the sub-grid scale reaction rate. These values can be related to the efficiency function $\mathscr{E}$ by:

$$\dot{\omega_{tot}} = \mathscr{E}\,\dot{\omega_{res}} = \frac{\mathscr{E}}{\mathscr{E}-1}\dot{\omega_{sgs}} \tag{7}$$

In areas where the flame in almost laminar (near the closed end of the chamber, before the second baffle plate), the flame wrinkling is fully resolved on the grid points and the contribution of the sub-grid scale combustion model is of course nearly 0%. On the other hand, in areas where the flame is fully turbulent, typically after the third grid, the resolved part of the combustion rate hardly reaches 25% of the total combustion rate. For the whole chamber and for the configuration 3 studied here, the mean ratio is 55%. This highlights the great importance of the sub grid-scale combustion model for this kind of simulation, as it has been shown by Di Sarli *et al.*,[15,16] even if the conditions are here very favorable to LES (well refined mesh and relatively "large" laminar flame

thickness compared to other fuels or other thermodynamic conditions). Values of the efficiency function $\mathscr{E}$ and thickening factor $\mathscr{F}$ averaged over the flame front for the different simulations performed are listed in Table. 1. These values are calculated at the time at which the flame wraps around the main central obstacle, i.e. when the flame is fully turbulent. It means that these values are representative of the maximum values obtained in the simulations. When going from CH_4 to C_3H_8 and to H_2, the global flame thickening factor increases as the laminar flame thickness decreases. The efficiency factor increases as well when going from CH_4 to C_3H_8 and to H_2. Indeed, when the laminar flame speed of the mixture increases, the flame propagation past the obstacles generates more turbulent structures, which will interact with the flame and makes it even quicker and more wrinkled. The sub-grid contribution of the combustion rate consequently becomes higher when going from CH_4 to C_3H_8 and to H_2. Finally, as expected, when the number of grids is increased, the turbulence level is increased and so the global efficiency factor.

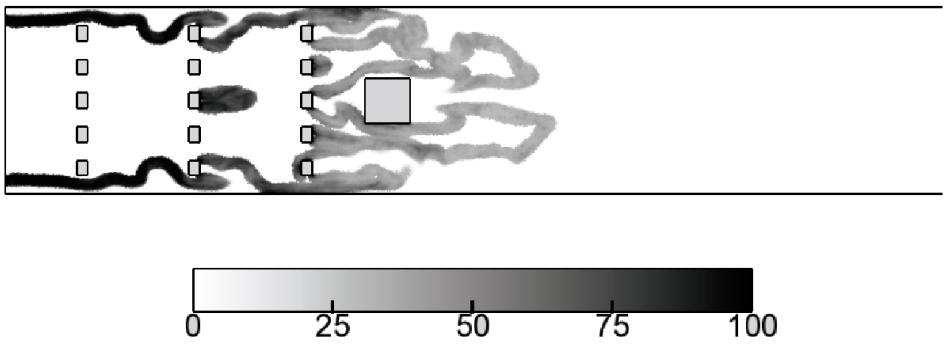

Figure 5: Resolved amount of reaction rate η Eq. 6- Config3 - C_3H_8

Table 1: Averaged values inside the flame front of thickening and efficiency factors.

	Thickening $\mathscr{F}$			**Efficiency $\mathscr{E}$**		
	Config1	**Config2**	**Config3**	**Config1**	**Config2**	**Config3**
CH_4	/	/	5,9	/	/	1,78
C_3H_8	7,2	7,2	7,2	1,38	1,67	1,84
H_2	/	/	21,5	/	/	1,94

A second way to characterize the quality of the LES is to quantify the amount of turbulent kinetic energy resolved. According to Pope's criterion,[30] LES should resolve 80% of the total turbulent kinetic energy. The contribution of the resolved part of the turbulent kinetic energy, ε, can be expressed:

$$\varepsilon = \frac{k_{res}}{k_{tot}} = 1 - \frac{k_{sgs}}{k_{tot}} \tag{8}$$

where k_{res} and k_{sgs} are respectively the resolved part and the sub-grid scale part of the total turbulent kinetic energy k_{tot}. The resolved turbulent kinetic energy k_{res} is defined as:

$$k_{res} = \frac{1}{2}(u_x'^2 + u_y'^2 + u_z'^2) \tag{9}$$

where u_x', u_y', and u_z' are the velocity fluctuations in each direction, expressed as:

$$u_i' = < U_i^2 > - < U_i >^2 \tag{10}$$

with U_i the resolved instantaneous velocity in direction i and $<>$ denoting time-averaging. The phenomenon studied here being transient, defining a time-averaging procedure to extract fluctuating values may be tricky. Here, following Di Sarli *et al.*,[15] a $0.1ms$ time interval has been chosen for time-averaging. This enables to minimize the variations of the mean fields due to the transient nature of the phenomenon, while the size of the data sample is kept sufficiently large to get meaningful statistics.

The sub-grid scale turbulent energy has been estimated from the sub-grid scale viscosity ν_{sgs}:[31]

$$k_{sgs} = \frac{1}{(C_m\Delta)^2}\nu_{sgs}^2 \tag{11}$$

where the constant C_m is defined as $C_m = \sqrt{2/3}A/(\pi K_0^{2/3})$. The coefficient $K_0 = 1.4$ corresponds to an infinite inertial spectrum for an homogeneous isotropic turbulence in the framework of Kolmogorov's hypothesis. The constant A is evaluated as A = 0.44 in the Eddy-Damped Quasi-Normal Markovian (EDQNM) theory.[32]

Figure. 6 shows the contribution of the resolved part of the turbulent kinetic energy in the flame front zone. In the most turbulent zones, after the turbulence generating grids, the criterion is fulfilled with about 100% of the total kinetic energy resolved. Close to the walls, at the closed end of the chamber, nearly 0% of the turbulent kinetic energy is resolved in the flame. However the amount of total kinetic energy in these areas is lower than 0.1% of the total kinetic energy in turbulent areas, showing that the level of turbulence in these areas is extremely low and the flame quasi laminar. This is corroborated by the results previously shown in Fig. 5. It can be consequently concluded that Pope's criterion is reasonably fulfilled, especially in areas where turbulence is a phenomenon of critical interest.

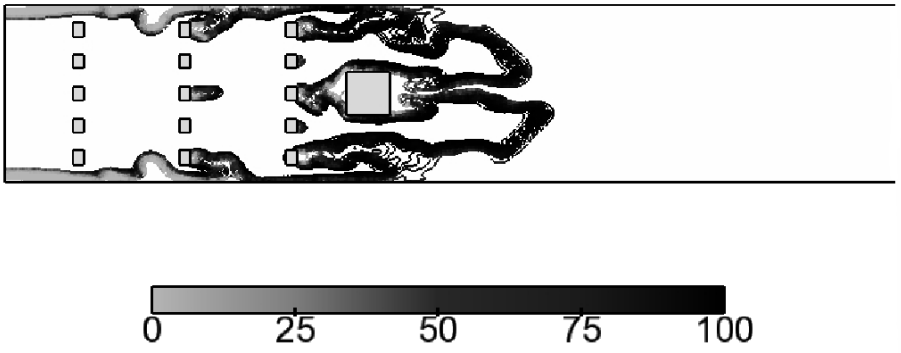

Figure 6: Contribution of the resolved part of the turbulent kinetic energy ε in the flame front - Config3 - C_3H_8

LES validation

The overpressure generated during the flame propagation is extracted from a probe located at the closed end of the chamber both in experiments and LES. It should be noted that due to the experimental variability on the timing between the different experimental realizations, experimental signals have been shifted in time in order to perform the averaging procedure and to extract mean signals and statistical envelopes. Consequently, validation of LES results will not be performed on a timing criteria but only on the magnitude and the trend of overpressure signals.

Figure 7 shows LES results relative to explosions performed with C_3H_8 for configurations 1 to 3 together with experimental mean signal and envelope of individual realizations. First, it can be noticed that LES is able to precisely reproduce the overpressure magnitude for any of the three configurations, from one to three turbulence generating grids. As mentioned earlier, post-maximum overpressure oscillations are as well correctly captured. The influence of the number of turbulence generating grids is also correctly reproduced: the flame is accelerated when adding grids and the resulting overpressure is consequently higher. This is mainly due to a higher global level of turbulence in the chamber as already mentioned by Masri *et al.*[9]

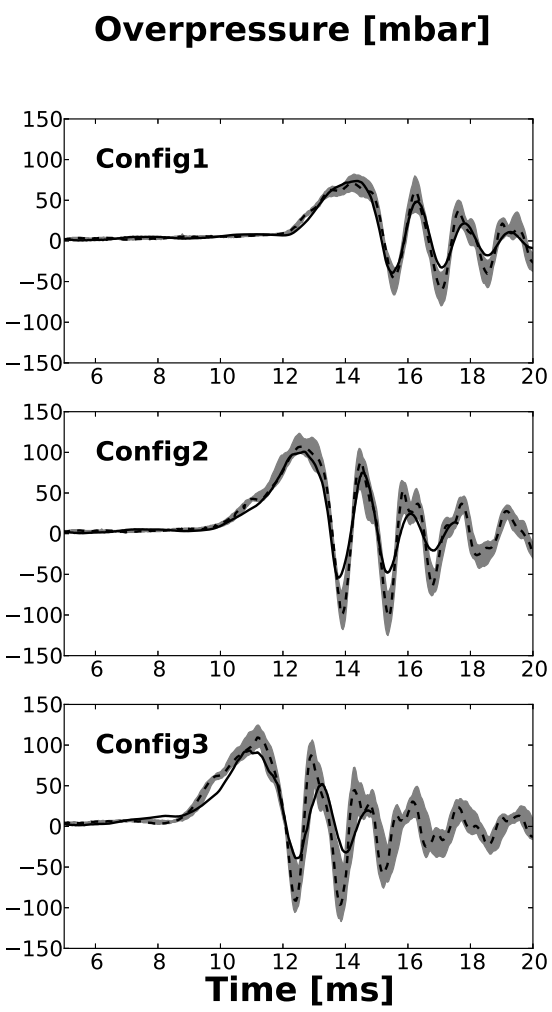

Figure 7: Comparison of overpressure signals between LES (plain) and experiments.[9] Mean signal (dashed) and statistical envelope (grey background) from 5ms to 20ms - C_3H_8 - Config 1, 2 and 3.

Figure 8 shows the results relative to the fuel influence for explosions performed in Config 3. Although Compressible Natural Gas (CNG) and Liquified Petroleum Gas (LPG) were used in experiments, these mixtures have been approximated by their main respective component in LES: CNG has been replaced by CH_4 (88% of CNG Volume) and LPG by C_3H_8 (95% of LPG volume). Once again, LES is also able to predict correctly the generated overpressure. C_3H_8 explosions generate higher overpressures than CH_4 ones. As shown experimentally by Masri *et al.*,[9] H_2, even at a lower equivalence ratio $\Phi = 0.7$, generates a much higher overpressure than C_3H_8 and CH_4. This can be mainly related to its higher laminar flame speed S_L^0 as shown in Table 2.

Table 2: Laminar flame speed for different fuels.

Fuel type	CH_4 at $\Phi = 1$	C_3H_8 at $\Phi = 1$	H_2 at $\Phi = 0.7$
S_L^0 **[cm/s] at** P_{atm}**, and** T_{atm}	36.3	38.4	128

These first results clearly show that LES seems an appropriate tool to deal with the multi-scale physics of explosion phenomena. Its ability to predict the critical parameters related to building safety issues has been shown:

- the maximum overpressure magnitude is correctly estimated;
- post-maximum pressure oscillations are captured;
- the influence of the obstacles is reproduced;
- the influence of the fuel type is reproduced.

Results sensitivity to LES sub-models

Although a large part of the overpressure is due to the turbulent character of the flame, it is highly influenced by the initial laminar propagation phase which controls the flame strength and shape before it hits the obstacles. This laminar phase is mainly controlled by chemical and thermo-diffusive small-scale effects. In the following, it is proposed to estimate the errors committed if rough sub-models are used to reproduce these effects. Two issues in particular are investigated:

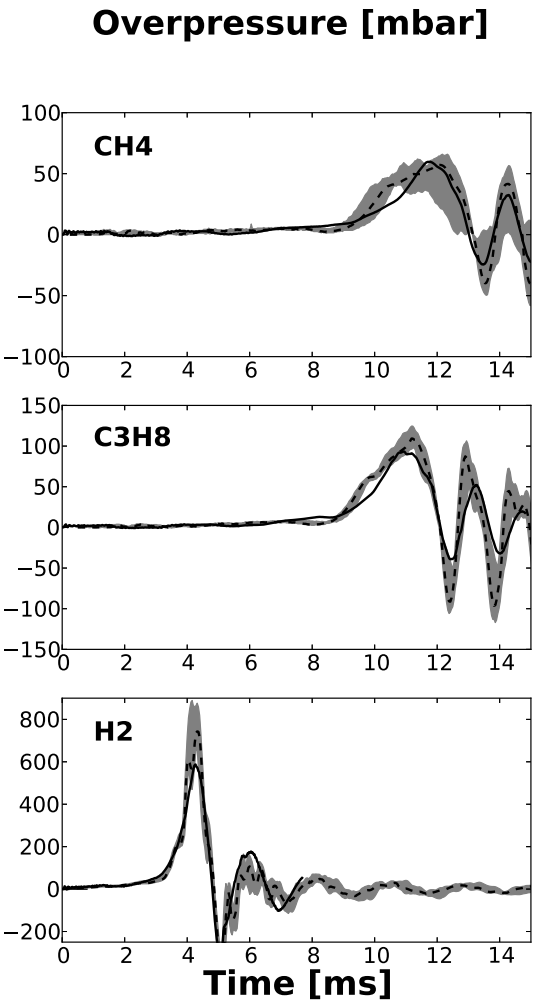

Figure 8: Comparison of overpressure signals between LES (plain) and experiments.[9] Mean signal (dashed) and statistical envelope (grey background) from 0ms to 15ms - Config 3 - CH_4, C_3H_8 and H_2.

- chemistry modeling;
- transport modeling.

Chemistry modeling influence

As mentioned earlier, the integration of detailed kinetics into turbulent flame simulations is impossible due to their prohibitive computational cost. Indeed, typical detailed mechanisms for C_3H_8-air combustion such as GRI-MECH 3.0[33] involve more than 50 species and 350 reactions. Tabu-

lated chemistry methods[34] have demonstrated their great potential to replace detailed kinetics.[35] However, these methods may become difficult to handle when dealing with complex industrial configurations[29] and curvature and strain effects (important in the laminar phase) can not be included easily. Another alternative solution is to use reduced chemical schemes.[29,36] In these methods, the number of species and reactions is reduced to the main ones with the minimum objective to reproduce the laminar flame speed and the adiabatic flame temperature at least. Reduced mechanisms are employed here for all calculations presented in this paper. In the results presented up to now, a 2-step mechanism (Table 3) has been used. This mechanism was built to reproduce the same laminar flame speed and burnt gases temperature than detailed mechanisms at $\phi = 1$, P_{atm} and T_{atm} (Table 5). Although the range of validity of this 2-step mechanism is restricted, it is adapted to this study since the flammable mixture is initialy perfectly premixed and pressure variations are too small to modify flame properties. However, in order to reduce the CPU cost, one could try to reduce even more the chemistry modeling to only one reaction: the fuel oxidation by O_2 (Table 4). However, when removing the CO-CO_2 equilibrium reaction, it is well known that the prediction of burnt gases temperature may become rough. Even though the 1-step mechanism has been built to give exactly the same laminar flame speed as the 2-step mechanism, it consequently overestimates the burnt gases temperature (Table 5).

Table 3: 2-step reduced mechanism for C_3H_8-Air combustion. Coefficients are related to the Arrhenius formulation of the reaction rate: $q = Ae^{\frac{-E_a}{RT}} \prod \left(\frac{\rho Y_k}{W_k}\right)^{n_k}$ where E_a is the activation energy of the reaction,W_k and n_k are respectively the molecular mass and reaction exponent for species k.

n	Reaction	A [$cm^3/mole.sec$]	Ea [cal/mole]
1	$C_3H_8 + 3.5O_2 \rightarrow 3CO + 4H_2O$ Forward : ${n_{C_3H_8}}^F = 0.55$ and ${n_{O_2}}^F = 0.9$	1.33E+012	4.15E+004
2	$CO + 0.5O_2 \leftrightarrow CO_2$ Forward : ${n_{CO}}^F = 1.0$ and ${n_{O_2}}^F = 0.5$ Reverse : ${n_{CO_2}}^F = 1.0$	4.5E+010	2.0E+004

Both C_3H_8-air schemes have been tested on Config 3 with our LES solver. The resulting over-

Table 4: 1-step reduced mechanism for C_3H_8-Air combustion.

n	Reaction	A $[\mathbf{cm^3/mole.sec}]$	Ea **[cal/mole]**
1	$C_3H_8 + 5O_2 \rightarrow 3CO_2 + 4H_2O$ Forward : ${n_{C_3H_8}}^F = 0.569$ and ${n_{O_2}}^F = 1.097$	3.09E+012	3.347E+004

Table 5: Chemistry mechanisms properties

Properties at $\Phi = 1$, P_{atm}, **and** T_{atm}	Laminar Flame Speed S_L^0 [m/s]	Burnt Gases Temperature T_{ad} [K]
Detailed mechanism (GRI-MECH[33])	38.4	2275
Reduced 2-step mechanism	38.4	2289
Reduced 1-step mechanism	38.4	2400

pressures are compared to the experimental data in Fig. 9 (left) and the flame front position (referred as the position of the furthest flame front point from ignition point) obtained with the two different kinetic mechanisms are shown in Fig. 9 (right). When the 2-step mechanism used up to now is replaced by the 1-step mechanism, the flame is accelerated and the overpressure is increased. The flame propagation speed S_d obtained with the 1-step mechanism is considerably higher than the one obtained with the 2-step mechanism all along the flame propagation. S_d is about 10% higher during the initial laminar phase and also during the turbulent propagation phase. Both propagation regimes are thus impacted, resulting in a 26% sensitivity of the overpressure to the chemical modeling. This result is directly related to the burnt gases temperature overestimation by the 1-step mechanism. Since the fresh to burnt gases density ration ρ_f/ρ_b is overestimated, the resulting flame propagation speed is overestimated,

$$S_d = \frac{\rho_f}{\rho_b} S_L^0 \tag{12}$$

and the generated overpressure as well. This shows that thermodynamics flame properties have a strong impact on global explosion parameters and should be correctly reproduced using an appropriate kinetic mechanism.

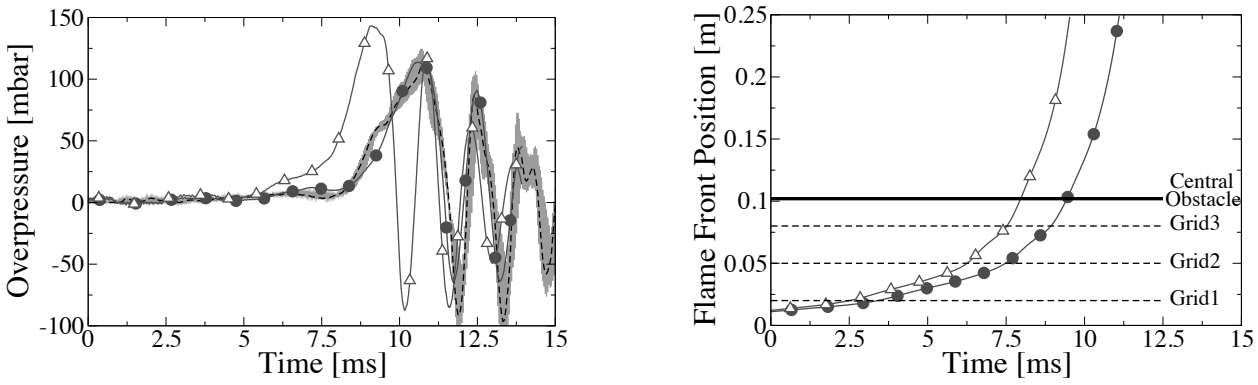

Figure 9: Influence of chemistry modeling - **Left:** Comparison of overpressure signals between LES and experiments.[9] 1-step mechanism LES (plain with triangles), 2-step mechanism LES (plain with circles), experimental mean signal (dashed) and statistical envelope (grey background). **Right:** Flame front position for LES calculations. 1-step mechanism LES (plain with triangles), 2-step mechanism LES (plain with circles) - Config 3 - C_3H_8.

Transport modeling influence

Knowing how fuel particles diffuse inside the mixture is characterized by its Lewis number Le_F. More generally, the Lewis number Le_k of any species k controls the competition between thermal and mass diffusion effects: $Le_k = \alpha_T / D_k$ where α_T and D_k are respectively the thermal and mass diffusivities. A common simplification when using reduced schemes in reactive CFD codes is to set Lewis numbers Le_k to one for all species, consequently neglecting the competition between thermal and mass diffusion but also neglecting preferential diffusion between the different species.

A second important consequence of this simplification is that the flame response to stretch is strongly modified. Indeed when the flame is stretched it can be shown that the consumption speed S_c (defined as the integral of the fuel burning rate across the flame front[27]) is strongly impacted. In the limit of small curvature terms, the consumption speed may be written as:[37,38]

$$\frac{S_c}{S_L^0} = 1 - L_a^c \frac{\kappa}{S_L^0} \tag{13}$$

where L_a^c is the Markstein length for the consumption speed and $\kappa = (1/S)dS/dt$ is the flame curvature with S the flame surface area.

This formulation is dependant on the Lewis number through L_a^c. Several expressions of L_a^c can be found in the literature. Clavin and Joulin[39] give:

$$L_a^c = \delta \frac{1}{2} \beta (Le_F - 1) \frac{T_f}{T_b - T_f} \int_0^{\frac{T_b - T_f}{T_f}} \frac{ln(1+x)}{x} dx \tag{14}$$

where T_b and T_f are respectively the burnt and fresh gas temperatures, and δ is the unstretched flame thickness. The parameter $\beta = (T_b - T_f)T_a/T_b^2$ measures the activation energy, with T_a the activation temperature.

Eq. 13 and Eq. 14 show that the Lewis number has a direct influence on the consumption speed when the flame is stretched. The consumption speed of a fuel with $Le > 1$ (such as C_3H_8) will therefore be significantly reduced for high curvatures, as it is typically the case in the early times after ignition. On the other hand, assuming that $Le = 1$ will lead to a zero value for the Markstein length and a flame speed independent of stretch to first order.

The burnt gases temperature T_b is also affected by stretch. In presence of stretch, the burnt gases temperature can be written as:[40]

$$\frac{(T_b - T_{ad})}{T_{ad}} = (\frac{1}{Le} - 1) \frac{D}{S_L^{0\,2}} \kappa \tag{15}$$

where D is a characteristic diffusivity. This shows that for a fuel with $Le > 1$, when the flame is stretched, the burnt gases temperature will be significantly reduced with regards to its adiabatic value T_{ad} for an unstretched flame. The $Le = 1$ assumption will lead to a burnt gases temperature independent of stretch. Using the simplification $Le = 1$ for a fuel whose actual Lewis number is larger than one, consequently leads to an overestimation of the burnt gases temperature which has for main consequence to overestimate the flame propagation speed as explained by Eq. 12.

In the results presented up to now a realistic transport model has been used in our calculations, i.e. a transport mechanism for which the response of the thickened flame to stretch is correctly reproduced. This can be easily done since the flame thickening is almost constant during the

whole computation and may be known a priori. In order to investigate the consequences of the $Le = 1$ simplification, another 2-step mechanism has been built (Table 6), replacing the transport model (used in the 2-step mechanism of Table 3) by a simplified transport for which the Lewis numbers Le_k have been set to one for all species. It should be noted that both mechanisms have been built to give exactly the same laminar flame speed and burnt gases temperature at $\phi = 1$, P_{atm} and T_{atm}.

Table 6: 2-step reduced mechanism with simplified transport for C_3H_8-Air combustion.

n	Reaction	A $[\mathbf{cm^3/mole.sec}]$	Ea [cal/mole]
1	$C_3H_8 + 3.5O_2 \rightarrow 3CO + 4H_2O$ Forward : ${n_{C_3H_8}}^F = 0.55$ and ${n_{O_2}}^F = 0.9$	1.41E+012	4.15E+004
2	$CO + 0.5O_2 \leftrightarrow CO_2$ Forward : ${n_{CO}}^F = 1.0$ and ${n_{O_2}}^F = 0.5$ Reverse : ${n_{CO_2}}^F = 1.0$	4.5E+010	2.0E+004

These two mechanisms have been tested on Config 3. The resulting overpressures are compared to the experimental data in Fig. 10 (left) and the flame front position obtained with the two different transport models are shown in Fig. 10 (right). When the realistic transport model is replaced by the simplified transport model, the flame is accelerated and the overpressure is overestimated. The flame propagation speed obtained with the simplified transport mechanism is higher than the one obtained with the realistic transport mechanism by a factor varying around 9% during the whole flame propagation. Both laminar and turbulent propagation phases are impacted. It means than even though the flow is largely turbulent during most part of the explosion, molecular and thermal transports are important and have a significant impact on the results. The consequence is a 23% sensitivity of the overpressure to the transport modeling.

This result is consistent with the conclusions which have been drawn from the theory: using the simplified transport model for C_3H_8-air combustion accelerates the flame because the effects of curvature on flame speed and burnt gases temperature are not captured. This overestimation of the flame propagation speed considerably modifies the flame dynamics and raises significantly the peak overpressure in the chamber. For CH_4 ($Le \sim 1$), further simulations have shown that, in

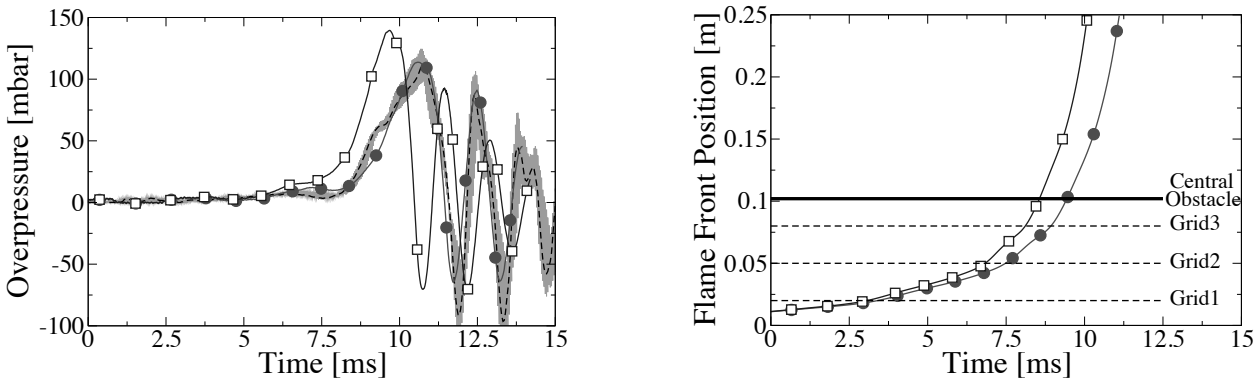

Figure 10: Influence of transport modeling - **Left:** Comparison of overpressure signals between LES and experiments.[9] Simplified transport mechanism LES (plain with squares), realistic transport mechanism LES (plain with circles), experimental mean signal (dashed) and statistical envelope (grey background). **Right:** Flame front position for LES calculations. Simplified transport mechanism LES (plain with squares), realistic transport mechanism LES (plain with circles) - Config 3 - C_3H_8.

agreement with the theory, the impact of such a modification is almost zero ($+0.05\%$). For H_2, the opposite behavior is observed, i.e. the flame propagation is slowed down and the overpressure is underestimated (-9%).

Although explosion processes are driven by turbulent combustion, the generated overpressure has been shown to be highly influenced by the initial laminar phase. A correct reproduction of this phase is a prerequisite to be able to precisely predict the overpressure increase inside the chamber. Even though thermodynamic and diffusive flame properties take place at very small scale, these effects must be correctly accounted for. This can be done using appropriate kinetic mechanisms and transport modeling.

Conclusion

The ability of LES to handle the multi-scale problem of gas explosion in a vented chamber has been shown. Explosion characteristic properties such as the maximum overpressure inside the chamber have been precisely reproduced. Geometric and fuel modification effects on the generated overpressure have been correctly captured as well. LES enabled to perform a diagnostic of explosions

in order to improve understanding of phenomena which drive them.

Even though LES seems a promising tool for explosion studies with higher predictive capacities compared to URANS, it remains very dependent on the quality of its sub-models and of the associated assumptions or simplifications. In this work, the strong influence of two LES sub-models have been highlighted. This shows that even though explosions are due to turbulent combustion processes, proper kinetic and transport modeling reproducing small-scale effects must be used in order to reproduce the correct initial laminar propagation phase which is crucial for the overpressure prediction.

Since the final objective of this work is to apply LES in real-size industrial buildings, it is now intended to extend the validity of these results to higher scale configurations. Scaled-up setups of the chamber studied in this paper are currently about to be studied experimentally and numerically to confirm these results.

Acknowledgment

This work was performed using HPC resources from GENCI-IDRIS. This work was supported by Total and ANRT under the CIFRE-2010-597. The authors thank Professor A. Masri (University of Sydney) for providing experimental data.

References

1. Bradley, D.; Mitcheson, A. The venting of gaseous explosions in spherical vessels. I–Theory. *Combust. Flame* **1978**, *32*, 221–236.

2. Dorofeev, S. B.; Bezmelnitsin, A. V.; Sidorov, V. P. Transition to detonation in vented hydrogen-air explosions. *Combust. Flame* **1995**, *103*, 243–246.

3. Bauwens, C. R.; Chaffee, J. L.; Dorofeev, S. B. Effect of Ignition Location, Vent Size, and

Obstacles on Vented Explosion Overpressures in Propane-Air Mixtures. *Combustion Science and Technology* **2010**, *182*, 1915–1932.

4. Dorofeev, S. B. Flame acceleration and explosion safety applications. *Proc. Combust. Inst.* **2011**, *33*, 2161–2175.

5. Hall, R.; Masri, A. R.; Yaroshchyk, P.; Ibrahim, S. S. Effects of position and frequency of obstacles on turbulent premixed propagating flames. *Combust. Flame* **2009**, *156*, 439–446.

6. Gubba, S. R.; Ibrahim, S. S.; Malalasekera, W.; Masri, A. R. LES modeling of premixed deflagrating flames in a small-scale vented explosion chamber with a series of solid obstructions. *Combust. Sci. Tech.* **2008**, *180*, 1936–1955.

7. Ibrahim, S. S.; Gubba, S. R.; Masri, A. R.; Malalasekera, W. Calculations of explosion deflagrating flames using a dynamic flame surface density model. *J. Loss Prev. Process. Indus.* **2009**, *22*, 258–264.

8. Di Sarli, V.; Di Benedetto, A.; Russo, G. Using Large Eddy Simulation for understanding vented gas explosions in the presence of obstacles. *J. Hazard. Mat.* **2009**, *169*, 435–442.

9. Masri, A. R.; Al-Harbi, A.; Meares, S.; Ibrahim, S. S. A Comparative Study of Turbulent Premixed Flames Propagating Past Repeated Obstacles. *Ind. & Eng. Chem. Res.* **2012**,

10. Di Benedetto, A.; Di Sarli, V.; Salzano, E.; Cammarota, F.; Russo, G. Explosion behavior of CH4/O2/N2/CO2 and H2/O2/N2/CO2 mixtures. *Int. J. Hydrogen Energy* **2009**,

11. Gubba, S. R.; Ibrahim, S. S.; Malalasekera, W.; Masri, A. R. Measurements and LES calculations of turbulent premixed flame propagation past repeated obstacles. *Combust. Flame* **2011**, *158*, 2465–2481.

12. Arntzen, B. J. Modelling of turbulence and combustion for simulation of gas explosions in complex geometries. Ph.D. thesis, Norwegian University of Science and Technology, Division of Applied Mechanics, Thermodynamics and Fluid Dynamics, 1998.

13. Zalosh, R. Explosion Venting Data and Modeling Literature Review. *The Fire Protection Research Foundation* **2008**,

14. Di Sarli, V.; Di Benedetto, A.; Russo, G.; Jarvis, S.; Long, E. J.; Hargrave, G. K. Large eddy simulation and PIV measurements of unsteady premixed flames accelerated by obstacles. *Flow, Turb. and Combustion* **2009**, *83*, 227–250.

15. Di Sarli, V.; Di Benedetto, A.; Russo, G. Large Eddy Simulation of transient premixed flame-vortex interactions in gas explosions. *Chemical engineering science* **2012**, *71*, 539–551.

16. Di Sarli, V.; Di Benedetto, A. Sensitivity to the Presence of the Combustion Submodel for Large Eddy Simulation of Transient Premixed Flame–Vortex Interactions. *Ind. & Eng. Chem. Res.* **2012**, *51*, 7704–7712.

17. Di Sarli, V.; Di Benedetto, A.; Russo, G. Sub-grid scale combustion models for large eddy simulation of unsteady premixed flame propagation around obstacles. *J. Hazard. Mat.* **2010**, *180*, 71–78.

18. Grout, R.; Gruber, A.; Yoo, C.; Chen, J. Direct numerical simulation of flame stabilization downstream of a transverse fuel jet in cross-flow. *Proc. Combust. Inst.* **2011**, *33*, 1629–1637.

19. Enaux, B.; Granet, V.; Vermorel, O.; Lacour, C.; Thobois, L.; Dugue, V.; Poinsot, T. J. Large Eddy Simulation of a Motored Single-Cylinder Piston Engine: Numerical Strategies and Validation. *Appl. Sci. Res.* **2011**, *86*, 153–177.

20. Boileau, M.; Staffelbach, G.; Cuenot, B.; Poinsot, T. J.; Bérat, C. LES of an ignition sequence in a gas turbine engine. *Combust. Flame* **2008**, *154*, 2–22.

21. Kolmogorov, A. N. The local structure of turbulence in incompressible viscous fluid for very large Reynolds numbers. *C. R. Acad. Sci. , USSR* **1941**, *30*, 301.

22. Gourdain, N.; Gicquel, L.; Montagnac, M.; Vermorel, O.; Gazaix, M.; Staffelbach, G.; Garcia, M.; Boussuge, J. F.; Poinsot, T. J. High performance parallel computing of flows in complex geometries: I. Methods. *Comput. Science & Discov.* **2009**, *2*, 015003.

23. Gourdain, N.; Gicquel, L.; Staffelbach, G.; Vermorel, O.; Duchaine, F.; Boussuge, J. F.; Poinsot, T. J. High performance parallel computing of flows in complex geometries: II. Applications. *Comput. Science & Discov.* **2009**, *2*, 015004.

24. Lax, P. D.; Wendroff, B. Difference schemes for hyperbolic equations with high order of accuracy. *Commun. Pure Appl. Math.* **1964**, *17*, 381–398.

25. Granet, V.; Vermorel, O.; Léonard, T.; Gicquel, L.; Poinsot, T. J. Comparison of nonreflecting outlet boundary conditions for compressible solvers on unstructured grids. *AIAA J.* **2010**, *48*, 2348–2364.

26. Ducros, F.; Nicoud, F.; Poinsot, T. J. Wall-Adapting Local eddy-Viscosity models for simulations in complex geometries. *Num. Meth. for Fluid Dynamics* **1998**, *1*, 293–300.

27. Poinsot, T. J.; Veynante, D. *Theoretical and Numerical Combustion*; R.T. Edwards, 3rd edition, 2012.

28. Colin, O.; Ducros, F.; Veynante, D.; Poinsot, T. J. A thickened flame model for large eddy simulations of turbulent premixed combustion. *Phys. Fluids* **2000**, *12*, 1843–1863.

29. Franzelli, B.; Riber, E.; Sanjosé, M.; Poinsot, T. J. A two-step chemical scheme for kerosene-air premixed flames. *Combust. Flame* **2010**, *157*, 1364–1373.

30. Pope, S. B. Ten questions concerning the large-eddy simulation of turbulent flows. *New Journal of Physics* **2004**, *6*, 35.

31. Sagaut, P. *Large eddy simulation for incompressible flows: an introduction*; Springer, 2005.

32. Aupoix, B.; Cousteix, J. Modèles simples de tension de sous-maille en turbulence homogène et isotrope. *La Recherche Aerospatiale* **1982**, *4*, 273–283.

33. Smith, G. P.; Golden, D. M.; Frenklach, M.; Moriarty, N.; Eiteneer, B.; Goldenberg, M.; Bowman, C. T.; Hanson, R. K.; Song, S.; Gardiner Jr, W. C. GRI-Mech 3.0 - `http://www.me.berkeley.edu/gri\_mech`. 1999.

34. Gicquel, O.; Darabiha, N.; Thévenin, D. Laminar premixed hydrogen/air counterflow flame simulations using flame prolongation of ILDM with differential diffusion. *Proc. Combust. Inst.* **2000**, *28*, 1901–1908.

35. Galpin, J.; Naudin, A.; Vervisch, L.; Angelberger, C.; Colin, O.; Domingo, P. Large-eddy simulation of a fuel-lean premixed turbulent swirl-burner. *Combust. Flame* **2008**, *155*, 247–266.

36. Westbrook, C. K.; Dryer, F. L. Simplified reaction mechanisms for the oxidation of hydrocarbon fuels in flames. *Combust. Sci. Tech.* **1981**, *27*, 31–43.

37. Bush, W.; Fendell, F. Asymptotic analysis of laminar flame propagation for general Lewis numbers. *Combust. Sci. Tech.* **1970**, *1*, 421.

38. Clavin, P. Dynamic behavior of premixed flame fronts in laminar and turbulent flows. *Prog. Energy Comb. Sci.* **1985**, *11*, 1–59.

39. Clavin, P.; Joulin, G. Premixed flames in large scale and high intensity turbulent flow. *Journal de Physique Lettres* **1983**, *44*, 1–12.

40. Law, C. K.; Cho, P.; Mizomoto, M.; Yoshida, H. Flame curvature and preferential diffusion in the burning intensity of bunsen flames. *Proc. Combust. Inst.* **1988**, *21*, 1803–1809.

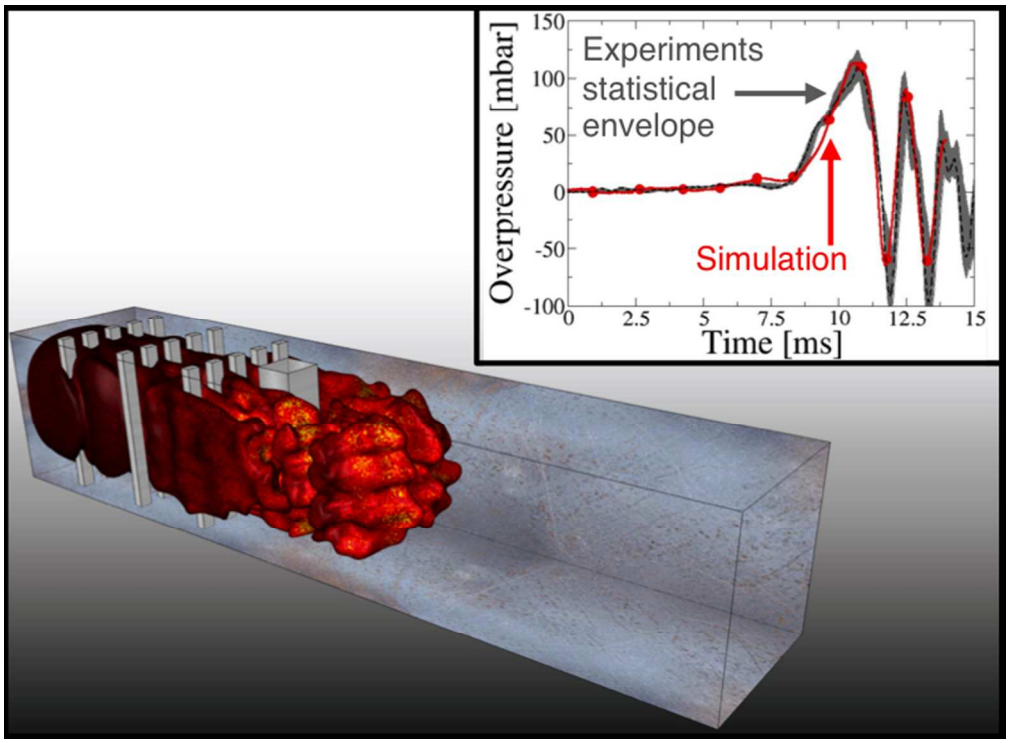

For table of content only: LES image of flame surface during propane-air deflagration and overpressure generated inside the chamber.
281x206mm (72 x 72 DPI)